Fast Thermal Characterization of Thermoelectric Modules Using Infrared Camera

Published Source
F. Attivissimo, A. Di Nisio, C. Calò Guarnieri Carducci, M. Spadavecchia "Fast Thermal Characterization of Thermoelectric Modules Using Infrared Camera " IEEE Transactions on Instrumentation and Measurement vol. 66, no. 2, pp. 305-314, February 2017, doi: 10.1109/TIM.2016.2631818

Manuscript number: **IM-16-12063R1**
Manuscript title: Fast Thermal Characterization of Thermoelectric Modules Using Infrared Camera

The publishing material is contained in the following sections:

- KEYWORDS and BROAD TOPIC
- MANUSCRIPT
- LIST OF FIGURES
- LIST OF TABLES
- LIST OF FIGURE CAPTIONS
- LIST OF TABLE TITLES
- SHORT BIOGRAPHIES

Authors' photographs and copyright form are in separate files.

No further changes to the manuscript have been requested by the reviewers and the associate editor.

KEYWORDS and BROAD TOPIC

Keywords:

Thermoelectricity,
Thermoelectric devices,
Thermal analysis,
Infrared imaging,
Thermal resistance

Broad Topic area:

14. Measurement of Materials and Applications

MANUSCRIPT

Fast Thermal Characterization of Thermoelectric Modules Using Infrared Camera

Filippo Attivissimo, *Member, IEEE*, Attilio Di Nisio, *Member, IEEE*, Carlo Guarnieri Calò Carducci, *Student Member, IEEE*, and Maurizio Spadavecchia, *Member, IEEE*

Department of Electrical and Information Engineering (DEI)
Politecnico di Bari
Via E. Orabona, 4 - 70125 Bari, Italy
[filippo.attivissimo, attilio.dinisio, carlo.guarniericalocarducci, maurizio.spadavecchia]@poliba.it

***Abstract* — Thermo-electric modules are receiving more and more attention due to the increasing interest in the energy harvesting sector. The selection of the proper module for a particular application can be done comparing the values of the figure of merit, which depends on electrical parameters such as internal electrical resistance and Seebeck voltage, and the equivalent thermal resistance. Although its importance, thermal resistance is more difficult to estimate than other parameters since well-engineered experimental setup is usually needed.**

In this paper, a new fast and non-invasive method based on thermal imaging techniques, to estimate the thermal resistance of thermoelectric modules, is presented. The comparison between this method and a direct measurement method based on thermocouple probes shows that very similar performance, with a small relative error, is achieved quicker, also avoiding to implement a complex measurement setup involving many temperature probes. Moreover, due to contactless nature of the procedure, the proposed experimental setup can be easily tuned for modules of different size without the need to modify any mechanical part.

***Index Terms*— Thermoelectricity, Thermoelectric devices, Thermal analysis, Infrared imaging, Thermal resistance**

I. Introduction

OVER the last years, the requirement of alternative energy solutions has become relevant to reach a sustainable development [1]. Thermo-electric modules (TEMs), are one of the proposed solutions, because of their capability to provide precision cooling when they are properly powered or to produce electric power when exposed to a temperature difference between their surfaces. These modules are receiving more and more attention due to the increasing interest in the energy harvesting sector [2][3], with applications such as efficiency improvement for autonomous sensors [4], energy autonomy of sensor nodes in Wireless Sensor Networks [5] [6], or also thermal energy recovery in those systems in which it would otherwise be dissipated. Another attractive challenge for researchers is electrical power generation to provide electricity and heat to spacecraft during long-time space exploration missions [7] or from low temperature heat sources and small temperature gradients [8].

The performance assessment of these modules plays an important role, either when they are used as thermoelectric coolers (TECs), or as thermoelectric generators (TEGs) [9]; for this reason, different techniques have been proposed to maximize the energy efficiency [10]. In the former case, they impact on the electrical power necessary to achieve a needed cooling power, whereas in the second one, they affect the entity of thermal energy that is converted into electricity. The use of TEG modules for recovering thermal energy is not new, however, because of their low efficiency, they have been generally used only in those contexts in which high thermal gradients were available, such as in the presence of heat generated by combustion engines [11] or compressors [12], thus making appreciable the energy contribution coming from the conversion. Indeed, although the total energy amount due to waste heat is very large, it is difficult to use it because of its inherent nature of low temperature and low energy density.

The application of new high efficiency thermoelectric materials has recently allowed operation with lower temperature gradient, as well as made possible cheaper production processes, thus TEG modules are finding new applications in consumer electronic devices, for example for recovering thermal energy produced by computer CPUs [13] or photovoltaic plants [14], but also as a possible energy source for powering the nodes in sensor networks once they are fully characterized from the consumption point of view [15] [16].

Scientific literature has recognized the figure of merit Z as a parameter that allows to compare the performance of different modules, independently of their geometrical dimensions [17][18]. Its expression takes into account both electrical parameters, such as the internal electrical

resistance and the Seebeck voltage, and thermal ones, such as the equivalent thermal resistance. Although its importance, thermal resistance is more difficult to estimate than other parameters since well-engineered experimental setup, involving a stack made by many measurement layers, is usually needed as widely explained in Section III. On the other end, especially for commercial modules, this parameter is commonly not reported in the datasheet.

With this work, the authors intend to propose a new fast and non-invasive method for TEMs thermal characterization based on thermal image processing, thus moving the complexity from the hardware to the software side, dramatically reducing the number of measurement layers.

This paper is structured as follows. After a theoretical review in Section II, a typical method to estimate the thermal resistance is described in Section III.A, which involves the measurement of four different temperatures between the surfaces of a reference material. The novel approach, described in Section III.B, is based on thermal imaging in order to obtain a temperature map of a ROI (Region of Interest) to quickly estimate the thermal resistance. In Section IV the testbed is drawn and detailed. Finally, in Section V results obtained with the new approach are compared with the classic one and confirmed by a further comparison with a third rough estimate based on the manufacturers' specification [19].

II. Theoretical Review

TEMs behavior is based upon three thermodynamically reversible effects, namely: Seebeck, Peltier and Thomson effects, which differ among them only because of the way they manifest themselves; but actually they all have a common ground and are related to the Seebeck coefficient.

A. Seebeck effect

This effect appears as an electromotive force $\boldsymbol{E}_{emf}$ in a material in response to a temperature gradient $\boldsymbol{\nabla} T$,

$$\boldsymbol{E}_{emf} = -s\boldsymbol{\nabla} T \tag{1}$$

where s is the absolute Seebeck coefficient, or thermoelectric power. Equation (1) is the basic principle for power generation in TEG modules. This voltage source extends the Ohm's law taking also into account the observable current in absence of measurable voltages. Its differential form is:

$$\rho \boldsymbol{J} = \left(-\boldsymbol{\nabla} V + \boldsymbol{E}_{emf}\right) \tag{2}$$

Integrating out equation (1), an expression of the voltage resulting on the terminals of a thermoelectric module in open circuit conditions is derived. For instance, when exposed to a temperature difference ΔT between its junctions, a TEG will exhibit a proportional voltage:

$$V_\alpha = \alpha \Delta T \tag{3}$$

where α is the relative Seebeck coefficient. More generally, when a TEM is supplied by a current, the measurable voltage is derived integrating out equation (2):

$$V = V_R + V_\alpha = R_{in} I + \alpha \Delta T \tag{4}$$

Equation (4) is composed by two different contributions: the voltage drop V_R on the internal resistance R_{in} and the thermoelectric one V_α. Equation (4) can be represented also as an equivalent electric circuit drawn in Fig. 8.

B. Peltier effect

It is the dual of the Seebeck effect; it appears when a current I flows in a junction of different conductors. This effect, characteristic of the TEC modules, induce a local heat flux q emitted or absorbed depending on the current direction

$$q = \Pi I = \alpha I T \tag{5}$$

where Π is the relative Peltier coefficient of the junction and T is its absolute temperature. The last term in (5) follows from the relation between the Seebeck and Peltier coefficients, i.e. $\Pi = \alpha T$.

C. Thomson effect

This plays a minor role because it is due to the Seebeck coefficient dependence with temperature, and appears as a distributed Peltier effect in a conductor exposed to a temperature gradient. Although it is an interesting physical topic, in many practical cases it is not taken into account since its effect is generally negligible if compared to the other ones. However, the relationship between α and the temperature T cannot be neglected in scenarios with very high temperature gradients because it affects the performance of TEG modules [20].

D. Figure of Merit Z

The thermoelectric figure of merit Z is a parameter which summarizes the bulk material proprieties and allows the comparison among TEM modules realized with different materials, dimensions and internal architectures. It is defined as

$$Z = \frac{\alpha^2 \Theta}{R_{in}} \tag{6}$$

Its expression (6) requires the knowledge of the relative Seebeck coefficient α, of the internal electrical resistance R_{in} and of thermal resistance Θ. Alternatively, the same meaning is given to a dimensionless parameter $Z\bar{T}$, where $\bar{T}$ is the average absolute temperature between the two surfaces of the module.

As a matter of fact, a TEM behaves like a heat engine (Fig. 1) that converts the electrical energy into thermal energy and vice versa according to the following relation:

$$|q_{em}| = |q_{abs}| + |VI|, \tag{7}$$

where, q_{em} and q_{abs} are respectively the emitted and absorbed heat flux from the surfaces of the module.

The figure of merit can thus be though as an indicator of

the conversion efficiency of energy processes involved, since its value grows as the electrical resistance decreases. In fact, all the three previously described physical processes are entirely reversible, conversely the energy dissipated by Joule effect on the internal resistance cannot be recovered. For this reason, the TEM conversion efficiency is the Carnot efficiency reduced by a factor which is function of the material's figure of merit [21]. Hence Z quantifies the ratio of thermoelectric effects to thermal effects, or equivalently of reversible to non-reversible processes.

Scientific literature includes different methods for the figure of merit assessment, which usually implies the use of different measurement principles for the determination of each parameter it is composed by. Many of them are inspired by the Harman method [22]-[25]. For example, one approach, known as *"modified Harman method"* [23], or *"Buist transient method"*, allows a direct estimation of Z with a single principle exploiting the different time constants of the electrical and thermal response. The main drawback of the cited method is that it is suitable only under specific conditions that cannot be obtained during normal operating conditions thus not allowing a full characterization of TEM modules. Generally, the Harman method is valid under the hypothesis of thermal equilibrium:

$$T_h \approx T_c \approx T_a \tag{8}$$

in particular, when temperature of the hot side T_h, the cold one T_c and ambient T_a do not deviate from the average $\bar{T}$ for more than $1/3$ of 1% [22].

This condition is typically achieved by injecting a pulsed current (see Fig. 2) large enough to be measured but sufficiently small to meet the condition (8) - generally in the order of milliamperes.

At steady-state, the current is switched on, which results in an immediate increase in voltage because the ohmic component of the voltage across the sample, V_R, appears. However, due to the slower characteristic response of heat transport compared to the electrical transport, a temperature difference still remains across the sample, generating a Seebeck voltage, with initial value V_R and final magnitude $V_R + V_\alpha$ according to equation (4). Then it can be proved [24] that the figure of merit $Z\bar{T}$ can be written as

$$Z\bar{T} = \left(1 + \frac{a\Theta}{2n}\right)\frac{V_\alpha}{V_R} \approx \frac{V_\alpha}{V_R} \tag{9}$$

where a is the thermal conductance from the surfaces of the module to the external medium. The term in brackets tends to unity when n (number of pellets in the module) is high.

When it is not possible to fulfill the condition (8), it is necessary to use the combination of several measurement methods to determine each of the three parameters as widely discussed in the literature, see for example [26]-[28].

III. Thermal Resistance Measurement

As already mentioned, among the three parameters of equation (6) the thermal resistance Θ results to be the less immediate to be measured, requiring a greater effort both in terms of number of temperature probes, as well as in the necessary readout electronics and mechanical parts for the realization of the measurement setup.

Before describing the method developed by the authors, it is convenient to find a suitable expression for the thermal resistance. Let start from the one-dimensional Fourier heat equation in steady state

$$q = -\kappa A \frac{dT}{dx} \tag{10}$$

where q is the heat flux, κ is the thermal conductivity, A is the cross-sectional area of heat flux path, dx and dT are respectively the infinitesimal increments in position and temperature in the flux direction. Integrating out (10), we can get a thermal equivalent of the Ohm's law (as suggested in [19]),

$$\Delta T = \Theta \cdot q \;\; \leftrightarrow \;\; V = R \cdot I \tag{11}$$

where Θ is the thermal resistance analogous to electrical resistance R, heat flux q and temperature difference ΔT are respectively analogous to the electric current I and voltage V at terminals.

It is therefore clear from (11) that the determination of Θ for any material requires the measurement of, at least, two different contributions (ΔT and q). In presence of an active element like a TEM, made by different coupled materials, it is not sufficient to estimate the heat flux on one surface only since the energy balance involves also the electrical power. Therefore, the emitted flux is equal to the absorbed one only if $|VI| = 0$; in all other cases it is necessary to determine the electrical power and both emitted and absorbed heat flux, thus acquiring four temperature measurements.

A. Direct method

Following the approach proposed in [26], both heat fluxes in (7), respectively q_{em} for the hot side and q_{abs} for the cold one, may be expressed as an energy balance between the Peltier effect, the heat conduction and Joule effect due to the injected current by

$$\begin{aligned} q_{em} &= \alpha I T_h - \frac{\Delta T}{\Theta} + \frac{I^2 R}{2} \\ q_{abs} &= \alpha I T_c - \frac{\Delta T}{\Theta} - \frac{I^2 R}{2} \end{aligned} \tag{12}$$

Considering the heat flux both emitted and absorbed by a TEC module, it is possible to derive the average heat flux $\bar{q}$ in order to eliminate the contribution due to the Joule effect

$$\bar{q} = \frac{(q_{em} + q_{abs})}{2} = \alpha I \frac{(T_h + T_c)}{2} - \frac{\Delta T}{\Theta} \tag{13}$$

where the heat fluxes may be determined using the scheme in Fig. 3, measuring four temperatures and using a reference medium with known thermal conductivity κ_{ref}.

It is

$$\begin{aligned} q_{em} &= \frac{\kappa_{ref} A (T_3 - T_4)}{L} = \frac{T_3 - T_4}{\Theta_{ref}} \\ q_{abs} &= \frac{\kappa_{ref} A (T_2 - T_1)}{L} = \frac{T_2 - T_1}{\Theta_{ref}} \end{aligned} \tag{14}$$

where A is the medium area, L is its thickness and $\theta_{ref} = L/(\kappa_{ref} A)$ is recognized as the known thermal resistance of the reference medium. Afterwards, T_h and T_c can be directly computed taking into account the temperature drop on ceramic surfaces of the TEC module.

$$\begin{aligned} T_h &= T_3 + q_{em}\Theta_{cer} \\ T_c &= T_2 + q_{abs}\Theta_{cer} \end{aligned} \tag{15}$$

where Θ_{cer} is the typical thermal resistance of the TEM ceramic surfaces.

Finally, solving (13) with respect to Θ, it is possible to derive a measurement formula for the unknown thermal resistance

$$\Theta = \frac{2\Delta T}{\alpha I (T_h + T_c) - (q_{em} + q_{abs})} \tag{16}$$

From (16), it is clear the need to measure more contributions, where α is supposed to have been previously estimated using another method, whereas I is the current injected into the module under test.

However, in addition to requiring four direct temperature measurement points with related thermal and mechanical coupling, as well as signal conditioning circuitry, this method is limited also by the need to adapt the measurement setup to different module sizes.

As better highlighted in Fig. 6, the setup is made by seven layers without considering the upper heat sink. In order to avoid any of the aforementioned difficulties, the authors proposal is to use a contactless method such as thermal imaging techniques to measure the temperature profile in two surrounding layers of the stack in Fig. 3, leading to a fast and extensive thermal characterization without any setup constrains. In this way the complexity is moved from the hardware to the software layer with the aim to reach good performance if compared to the direct method.

B. Thermal Imaging method

In the last forty years the use of thermal imaging cameras has attracted strong interest of the industry and of many researchers becoming a useful tool for industrial applications [29], military [30], medical diagnosis [31] and for contactless measurements [32]. This approach is particularly suitable to provide large contiguous sets of surface temperatures data thus it can be used in several applications, like: to validate heat flow models [33], to thermally characterize electronic chip packages [34] or to study thermal stresses induced in different devices alongside other reliability techniques [35]-[38]. In particular, in [39], thermal imaging is used with electrical measurements to evaluate the effect of thermal cycling on TEMs studying mechanical failures and degradation of figure of merit and its components.

Infrared measurements do not need a direct heat conduction between the object to be measured and the probe, but they rather rely on radiated energy. To correctly understand thermal images, different factors have to be considered such as the physics of the device under test and the non-uniformity of temperature.

Every object emits a total thermal radiation W which depends on its own temperature T according to the Stefan-Boltzmann law

$$W = \varepsilon W_e = \varepsilon \sigma T^4 \tag{17}$$

where $\sigma = 5.67 \cdot 10^{-8}\ [\mathrm{W/m^2K^4}]$ is the Stefan-Boltzmann constant, W_e is the power emitted from a black-body and ε is the emissivity of a grey-body ranging from 0 to 1.

However, thermal cameras are generally based on detectors particularly sensitive to a bandwidth around a specific wavelength λ_p dependent on their physical characteristics. Hence only a part of W is detected and can be computed taking into account the spectral radiance of the body near λ_p and the spectral sensitivity of the detectors. For a black body at absolute temperature T the spectral radiance as a function of wavelength λ is given by Planck's law

$$W_{\lambda e}(\lambda) = \frac{2\pi h c^2}{\lambda^5 \left(e^{\frac{hc}{\lambda k_B T}} - 1 \right)} \tag{18}$$

where h is the Planck constant, c is the light speed in vacuum and k_B is the Boltzmann constant.

Moreover, it is necessary to consider that the total radiation measured by the camera is not due exclusively to the one directly emitted from the object W_{obj}, but is also composed of two additional contributions, the radiation emitted by the atmosphere W_{atm} and the one reflected from surrounding objects W_{refl} (Fig. 4). All these contributions are in turn affected by the influence of the emissivity ε and of the atmosphere transmittance τ; the latter value depends mainly on the object distance, on the atmospheric temperature and on relative humidity [40].

Hence, the total incident radiation W_{tot} on the detector may be expressed as sum of all cited contribution

$$W_{tot} = \varepsilon \tau W_{obj} + (1 - \varepsilon)\tau W_{refl} + (1 - \tau) W_{atm}\,. \tag{19}$$

The equation (19) is typically implemented inside thermal cameras, but can also be used to make a system calibration by calculating a proper emissivity value for an object [40]. If we assume to know the emissivity ε_1 of an object for which we measure a temperature T_{obj_1} via thermal imaging and we measure for the same object also a temperature T_{obj_2} using a more accurate method, then a new value of emissivity ε_2 can be derived by imposing that the resulting total radiation incident on the detector are equal

$$\begin{cases} W_{tot} = \varepsilon_1 \tau W_{obj_1} + (1-\varepsilon_1)\tau W_{refl} + (1-\tau) W_{atm} \\ W_{tot} = \varepsilon_2 \tau W_{obj_2} + (1-\varepsilon_2)\tau W_{refl} + (1-\tau) W_{atm} \end{cases} . \quad (20)$$

Substituting (17) in (20), and subsequently solving for ε_2, we derive

$$\varepsilon_2 = \varepsilon_1 \frac{T_{obj_1}^4 - T_{refl}^4}{T_{obj_2}^4 - T_{refl}^4} \quad (21)$$

with values constrained to range $\varepsilon_2 \in [0,1]$. A similar result could have been obtained using (18), evaluated in $\lambda = \lambda_p$, instead of (17) [41] [42].

Once the thermal image of the profile sketched in Fig. 3 has been acquired, the temperatures measured at the interfaces can be substituted in (14) and (16), as is done in the direct method, leading more quickly to the same result. However, since in this case, we do not deal with simple measurement points but rather with an array of pixels, it is necessary to perform a preliminary step to identify the pixels corresponding to the interfaces between the medium.

The technique is based on the assumption that the temperature is uniform along the x-axis within a limited ROI. This ROI can be thought composed by M layers each of thickness h_l (with $l = 1, \dots, M$) thus the whole stack has a height $H_T = h_1 + \cdots + h_M$. The ordinates, in the image reference frame, of the lower and upper surface of the l-th layer are denoted as y_{l-1} and y_l, respectively. Fig. 5 shows the thermal profile and the ROI for a simulated stack of materials similar to the one sketched in Fig. 3.

Let $T(x,y)$ be the digital image and $(x_0 - \Delta x/2\,, y_0)$, $(x_0 + \Delta x/2, y_M)$ the opposite corners of the rectangular ROI of width Δx and height $\Delta y = y_M - y_0$. In order to measure the vertical temperature profile inside the ROI, all the temperature values are averaged along the x-axis direction. In this way the image array $T(x,y)$ is reduced to a vector $T_{\bar{X}}(y)$,

$$T_{\bar{X}}(y) = \frac{1}{\Delta x + 1} \sum_{x \in \bar{X}} T(x,y) \quad , y \in Y \quad (22)$$

where $\bar{X} = \{x: x_0 - \Delta x/2 \le x \le x_0 + \Delta x/2\}$ and $Y = \{y:\ y_0 \le y \le y_M\}$.

Since the thickness of each layer of the stack is already known, the position of their interfaces in the image is easily obtained from y_0 and y_M through a simple proportion. Hence the values y_0 and y_M should be determined carefully, with the procedure described later. In particular, it is possible to obtain the value of the ordinates in the image corresponding to the interfaces between layers as

$$y_l = y_0 + (y_M - y_0) \sum_{m=1}^{l} k_m \,. \quad (23)$$

where the quantities k_l, defined as,

$$k_l = \frac{h_l}{H_T}, \quad l = 1, \dots M \quad (24)$$

form a vector $K_T = [k_1, \dots k_M]$ which contains the geometric normalized structure of the stack. For instance, applying (23) to the scheme in Fig. 3, we can derive the temperature at the interfaces

$$\begin{aligned} T_1 &= T_{\bar{X}}(y_0) = T_{\bar{X}}(y_0) \\ T_2 &= T_{\bar{X}}(y_1) = T_{\bar{X}}(y_0 + \Delta y \cdot k_1) \\ T_3 &= T_{\bar{X}}(y_2) = T_{\bar{X}}\big(y_0 + \Delta y \cdot (k_1 + k_2)\big) \\ T_4 &= T_{\bar{X}}(y_3) = T_{\bar{X}}\big(y_0 + \Delta y \cdot (k_1 + k_2 + k_3)\big) \,. \end{aligned} \quad (25)$$

The determination of y_0 and y_M is carried out using a least squares method. However, in order to overcome the low resolution limit of the adopted camera and get a higher precision in layers detection, the vertical temperature profile $T_{\bar{X}}$ is first oversampled of a factor 50. Indeed, substituting (25) into (14) and using the relation (7), y_0 and y_M are obtained minimizing the error between the power drained by the TEC module, estimated as difference between the emitted and absorbed heat flux $\Delta q = q_{em} - q_{abs}$, and the measured supplied power $P = VI$

$$\underset{[y_0, y_M]}{\operatorname{argmin}} \frac{\|e\|_2}{\sqrt{N_s}} = \underset{[y_0, y_M]}{\operatorname{argmin}} \frac{\|\Delta q - P\|_2}{\sqrt{N_s}} \quad (26)$$

with N_s the number of sampled points.

IV. Automatic Test Bench

In order to validate the proposed method, the thermal resistance of a TEC module was estimated with both the proposed method and the direct one comparing the obtained results. For this purpose, the authors developed the experimental setup in Fig. 6 to allow simultaneous measurements of the temperature profile with both methods varying the applied voltage, i.e. the injected current I, and measuring the generated temperature gradient ΔT. The TEC under test is a common commercial low-cost module TES1-12730 from Thermonamic Electronics Corporation [43], having the parameters reported in TABLE I.

The module under test is placed between two identical heat flux sensors each one obtained interposing a glass layer (with thickness h_{glass}) between two aluminum plates (with h_{alu} thickness) in which a type J thermocouple has been inserted to read the local temperature at the interfaces. Each contact surface was dressed with a thermal conductive paste in order to minimize thermal losses.

It was worth noting that the aluminum plates are a

necessary complication used only to compare the reference method with the proposed one which required only the thermal image of a stack similar with the one reported in Fig. 3 made by only three layer instead of the seven required for thermocouples-based measurements.

For the sake of completeness, values for all geometrical and physical parameters are summarized in TABLE II.

The entire stack is thermally insulated along sides by a properly shaped polystyrene block, leaving only a small window to take the thermal images. The thermal exchange between the outer surfaces and the room is established thanks to two aluminum heat sinks air cooled with fans. As long as the temperature varies, voltages generated by thermocouples are directly acquired at 10 kS/s by a 16-bit DAQ board X Series USB 6361 by National Instruments and then averaged over one second. A software cold-junction compensation is then applied using an integrated temperature sensor, model LM35 from Texas Instruments, previously calibrated in a Discovery Es 250 (DY-250) climatic chamber from Angelantoni Group S.p.A..

The whole characterization process is handled by MATLAB and a routine based on the Robot class from Java platform has been specifically designed for automating thermal image capturing. A T335 FLIR thermal imaging camera was used, placed at a distance d from the setup. The robot (Fig. 7) controls the mouse over the FLIR ResearchIR™ 4 [44] software window and simulates keys pressed on the keyboard in order to export the thermal image in MATLAB format as a temperature matrix, averaged over 16 frames, for further processing.

As reported in Fig. 8, the TEC under test is powered by a 4-quadrant amplifier Toellner TOE7621, driven by a voltage signal from an Agilent 33220A arbitrary function generator controlled through IEEE 488 bus. Two Agilent 34401A multimeters, interfaced also via IEEE 488 bus, are used to measure the current I absorbed by the module and the voltage V at its terminals in order to calculate the power consumption P.

The test procedure, summarized in the flow chart in Fig. 7, is iterated for 10 different voltage values from $V = 400\,\text{mV}$ to $V = 4\,\text{V}$ in order to perform a thermal characterization of the module for different steady state operating conditions. After the voltage changes and before starting to acquire signals a pause time of five times the TEC module thermal time constant (5τ) is waited. In this way it is possible to ensure that the test starts after the achievement of steady state conditions and all transient behaviors are vanished. The value of τ was calculated identifying the TEC thermal model by an Autoregressive Exogenous (ARX) method included in MATLAB System Identification Toolbox. For this specific case, the model was identified obtaining the 91.19% Normalized Root Mean Squared Error [45]; the time constant is the greatest value among $\tau_{32} = 9.73$ s, referred to output ΔT_{32} at TEC surfaces, and $\tau_{41} = 72.3$ s, referred to output ΔT_{41} at stack extremities, obtaining a steady state temperature variation below 0.7%.

V. Experimental Results

A comparison between the proposed method and the thermocouple based one was performed over the ten values of the voltage driving the TEC.

Before presenting the measured thermal profiles, it is important to describe how the emissivity setting of the thermal camera was obtained. Indeed, as it is clear from the Fig. 6, in the Field of View of the thermal imaging camera materials are stacked that have very different emissivity values, ranging from 0.92-0.94 for smooth glass to less than 0.3 for aluminum. Therefore, in order to obtain a uniform emissivity map, a strip of black electrical tape (IEC60454-3-1-5/F-PVCp/90) was attached along the stack (see [46]), whose emissivity value was derived as follows.

1) We first attached a TP878 Pt100 contact probe by Delta OHM to a polished aluminum surface which is placed to cover the pointed ROI. The camera was configured so that $\varepsilon = 1$ and temperature measurements are averaged over 16 frames.

2) The camera was used to measure the temperature T_{refl} reflected on the surface over a ROI of 23x23 pixels.

3) Hence, a strip of electrical tape was put on the metal surface and, after assuming a typical emissivity $\varepsilon_1 = 0.95$, it was measured the target temperature T_{obj1} over the same ROI. At the same time, the target temperature T_{obj2} was also acquired using the Pt100 probe with a numbers of samples N equal to the number of pixels in the camera ROI.

4) In a final calculation step, we substituted the N samples of T_{obj1}, T_{obj2} and T_{refl} in the equation (21), so obtaining N values for ε_2, with mean value $\bar{\varepsilon_2} = 0.918$ and standard deviation $\sigma_{\varepsilon_2} = 0.007$. Thus the value $\varepsilon_{cal} = 0.92$ was used in all the subsequent tests.

For sake of clarity, it is important to bear in mind that this new emissivity value does not claim to represent an absolute estimation of the emissivity of the electrical tape used, but rather the calibration factor of the thermal imaging method with respect to the Pt100 reference method, taking into account several factors like the setup geometry, the ambient temperature and last but not least the target emissivity.

The resulting temperature profiles for several currents I are reported in Fig. 10. Each profile was obtained averaging horizontally the masked image shown in Fig. 9.

The importance of using the black tape to get a uniform emissivity map appears clear if we compare the temperature profile of the taped and untaped measurement box. In the latter case, because of the low emissivity of the aluminum layers, the measured temperature of that layers tends to the reflected one, as evinced from Fig. 11.

In order to compute the heat flux, equation (15) should

be modified in (27) to take also into account the temperature drops on the aluminum layers. Indeed, T_3 and T_2 from Fig. 10 are related to the temperature at the interface glass/aluminum and not aluminum/TEC.

$$\begin{aligned} T_h &= T_3 + q_{em}(\Theta_{cer} + \Theta_{alu}) \\ T_c &= T_2 + q_{abs}(\Theta_{cer} + \Theta_{alu}) \end{aligned} \tag{27}$$

Since the knowledge of the value of the Seebeck coefficient is required for the computation of the thermal resistance, we used the procedure described in [19] to derive both the value of α_{ds} and the expected value of thermal resistance Θ_{ds} from the module datasheet. See TABLE I.

Experimental results reported in Fig. 12 show a good agreement in heat fluxes measurements between the thermocouple based method and the proposed one. Conversely, a greater difference arises in the determination of the thermal resistance, since expression (16) involves also absolute temperatures. As evinced from Fig. 13, the relative error is greater for $\Delta T < 10$ °C, because of the low accuracy of the thermocouples measurements when the sensing junction is at a temperature near to the cold junction one. In any case, the thermal resistance is underestimated with respect to the direct measurement method with a typical relative error around 2%. In order to further validate the proposed method, it is possible to observe that the obtained thermal resistance is compatible with the approximate estimate Θ_{ds} reported in TABLE I.

Finally, repeated experiments were performed with a twofold objective: *i)* to quantify the short-term stability of the thermal camera and consequently the temperature matrix in the ROI and *ii)* to compare, more interestingly, the precision of the proposed method with respect to the thermocouple based one.

In order to have a good comparison of the two methods, the test was made at best condition for the thermocouples, i.e. for measured temperatures far enough from the cold-junction temperature; in other words, this condition corresponds to the highest stimulus voltage (i.e. 4 V) which induce a temperature drop $\Delta T \approx 30$ °C between the surfaces of the TEM.

In TABLE III are reported the results obtained for 90 repetitions without changing any parameter. By comparing all the obtained standard deviations, it is clear that the dispersion of each value is in the same order of magnitude for both methods with a slight advantage for the reference method. Without considering the other benefits introduced with the thermal imaging, which have been previously discussed, this result further confirms the goodness of the proposed approach. Statistics in fact show that, after performing an accurate calibration, the achievable performance of thermal imaging based methods are comparable with direct ones.

VI. Conclusion

In this work, a new fast method to estimate the thermal resistance of TEM modules was presented. The novelty consists in using a thermal image processing technique to obtain a temperature profile of the stacked setup in each working condition while a segmentation procedure let to estimate the temperature at the interfaces overcoming the limited resolution of the thermal camera and reducing the number of measurement layers needed. Direct and thermal imaging temperature measurements let us to obtain two different estimation of heat fluxes and then of thermal resistance; such estimations have been compared showing a slight underestimation of the proposed method with respect to the direct one. Finally, the evaluation of the repeatability of both methods has been performed and the results reported in Section V showing the suitability of using contactless thermal imaging techniques to achieve a small error in thermal resistance assessment if compared to a thermocouple based method and to a datasheet-based estimation, without the need of using and designing complex measurement testbed which commonly involves many probes and fiddly circuitry.

References

[1] A. Malik and E. Grohmann, Eds., Enviromental Protection Strategies for Sustinable Development, New York, NY, Usa, Springer-Verlag, 2012.

[2] M. Lallart Eds., Small-Scale Energy Harvesting, *InTech open acess books*, 2012.

[3] S. Dalola, M. Ferrari, V. Ferrari, M. Guizzetti, D. Marioli, and A. Taroni, "Autonomous sensor system with power hearvesting telemetric temperature measurement of pipes", *IEEE Trans. Instrum. Meas.*, vol. 58, no. 5, pp. 1471-1478, May 2009.

[4] S. Dalola, M. Ferrari, V. Ferrari, M. Guizzetti, D. Marioli, and A. Taroni, "Characterization of thermoelectric modules for powering autonomous sensors", *IEEE Trans. Instrum. Meas*., vol. 58, no. 1, pp. 99-107, January 2009.

[5] F. Adamo, F. Attivissimo, C. Guarnieri Calò Carducci, A.M.L. Lanzolla, "A Smart Sensor Network for Sea Water Quality Monitoring, *IEEE Sensors Journal*, vol. 15, no. 5, pp. 2514-2520, May 2015.

[6] I. Korhonen, R. Lankinen, "Energy harvester for a wireless sensor in a boiler environment, *Measurement*, Volume 58, December 2014, Pages 241-248, ISSN 0263-2241, doi: j.measurement.2014.08.037

[7] G. Andria, G. Cavone, C. Guarnieri Calò Carducci, M. Spadavecchia, "A PWM Temperature Controller for Themoelectric Generator Characterization", in *Metrology for Aerospace (MetroAeroSpace), 2016 IEEE*, Firenze, pp. 295-300, May 2016.

[8] S. E. Jo, M. K. Kim, M. S. Kim and Y. J. Kim, "Flexible thermoelectric generator for human body heat energy harvesting," in *Electronics Letters*, vol. 48, no. 16, pp. 1013-1015, August 2 2012. doi: 10.1049/el.2012.1566

[9] S. LeBlanc, S. K. Yee, M. L. Scullin, C. Dames, k. E. Goodson, "Material and manufacturing cost consideration for thermoelectrics", *Renewable Sustainable Energy Rev.,* vol. 32, pp. 313-327, April 2014.

[10] M. Chen, "Distributed detection and control of thermoelectric generator modules using sensors nodes", *IEEE Trans. Instrum. Meas.*, vol. 63, no. 1, pp. 191-202, January 2014.

[11] V. Sandu, A. Stanca, A. Pasaroiu, D. Dobre, "Experimental investigation of thermoelectric heat recovery from a diesel engine", *2012 International Conference on Applied and Theoretical Electricity (ICATE)*, 2012, pp. 1-8, doi: 10.1109/ICATE.2012.6403406

[12] E. Navarro-Peris, J. M. Corberan, Z. Ancik, "Evaluation of the potential recovery of compressor heat losses to enhance the

efficiency of refrigeration systems by means of thermoelectric generation", *Applied Thermal Engineering*, Volume 89, 5 October 2015, Pages 755-762, ISSN 1359-4311, doi: j.applthermaleng.2015.06.033.

[13] G. L. Solbrekken, K. Yazawa and A. Bar-Cohen, "Heat driven cooling of portable electronics using thermoelectric technology," in *IEEE Transactions on Advanced Packaging*, vol. 31, no. 2, pp. 429-437, May 2008. doi: 10.1109/TADVP.2008.920356

[14] F. Attivissimo, A. Di Nisio, A.M.L Lanzolla, M. Paul, "Feasibility of a Photovoltaic–Thermoelectric Generator: Performance Analysis and Simulation Results," *IEEE Transactions on Instrumentation and Measurement*, vol.64, no.5, pp.1158,1169, May 2015. ISSN 0018-9456. DOI:10.1109/TIM.2015.2410353

[15] P. Dziurdzia, J. Stepien, "Autonomous wireless link powered with harvested heat energy", *2011 IEEE International Conference on Microwaves, Communications, Antennas and Electronics System (COMCAS)*, 2011, pp, 1-4, doi: 10.1109/COMCAS.2011.6105890

[16] A. Di Nisio, T. Di Noia, C. Guarnieri Calò Carducci, M. Spadavecchia, "High Dynamic Range Power Consumption Measurement in Microcontroller Based Applications," *IEEE Transactions on Instrumentation and Measurement*, DOI: 10.1109/TIM.2016.2549818, to be published.

[17] D. Mitrani, J. A. Tomé, J. Salazar, A. Turò, "Methodology for extracting thermoelectric module parameters", *IEEE Trans. Instrum. Meas.*, vol. 54, no. 4, pp. 1548-1552, August 2005.

[18] D. M. Rowe, G. Min, "Evaluation of thermoelectric modules for power generation", *Journal of Power Source*, vol. 73, no. 2, pp. 193-198, June 1998.

[19] S. Lineykin and S. Ben-Yaakov, "Modeling and Analysis of Thermoelectric Modules," in *IEEE Transactions on Industry Applications*, vol. 43, no. 2, pp. 505-512, March-april 2007. doi: 10.1109/TIA.2006.889813

[20] B. T. Admasu and X. Luo, "Effects of thermal contact resistance and Thomson heating on the outputs of solar thermoelectric power generation system," *14th International Conference on Electronic Packaging Technology (ICEPT)*, 2013, Dalian, 2013, pp. 1260-1263. doi: 10.1109/ICEPT.2013.6756686

[21] K. Hee Seok, L. Weishu, C. Gang, C. Ching-Wu, R. Zhifeng, "Physics Relationship between thermoelectric figure of merit and energy conversion efficiency", *Proc Natl Acad Sci USA*. 2015 Jul 7; 112(27): 8205–8210. doi: 10.1073/pnas.1510231112

[22] T. C. Harman, J. H. Cahn, M. J. Logan, "Measurement of Thermal Conductivity by Utilization of the Peltier Effect", in *Journal of Applied Physics 30*, 1351 (1959); doi: 10.1063/1.1735334.

[23] R. J. Buist, "Methodology for testing thermoelectric materials and devices", in *CRC Handbook of Thermoelectrics*, D. M. Rowe, Ed. Boca Raton, FL: CRC, 1995, pp. 189–209.

[24] G. Gromov, D. Kondratiev, A. Rogov, L. Yershova., "Z-meter: Easy-to use Application and Theory," *Proceedings. Sixth European Workshop on Thermoelectricity of the European Thermoelectric Society Freiburg* im Breisgau, September 20-21, 2001.

[25] H. Iwasaki and H. Hori, "Thermoelectric property measurements by the improved Harman method," *ICT 2005. 24th International Conference on Thermoelectrics*, 2005, pp. 513-516. doi: 10.1109/ICT.2005.1519995

[26] T. A. Ajiwiguna, A. Ismardi, S. Y. Kim, "Measurement System for Thermoelectric Module", *IEEE I2MTC 2015 Proceedings*, 2015

[27] H.J. Kim, J. R.Skuza, P. Yeonjoon, G.C. King, S.H. Choi, A. Nagavalli, "System to Measure Thermal Conductivity and Seebeck Coefficient for Thermoelectrics", *NASA Lancgley Research Center Technical Memorandum*, NASA/TM-2012-217791

[28] M.K. Russel, D. Ewing, C.Y. Ching, "Characterization of a thermoelectric cooler based thermal management system under different operating conditions", *Applied Thermal Engineering*, Elsevier, 2012, doi:10.1016/j.applthermaleng.2012.05.0027

[29] M. Vollmer, K. P. Mollmann, *Infrared Thermal Imaging: Fundamentals, Research and Applications*, New York, NY, Usa, Wiley, 2010.

[30] A. Rogalski, "Recent progress in infrared detector technologies", *Infrared Phys. Technologies*, vol. 54, pp. 136-154, April 2011.

[31] E. J. Ring, K. Ammer, "Infrared thermal imaging in medicine", *Journal of Physiological Measurement*, vol. 33, pp. 33-46, April 2012.

[32] G. Andria, A. Bruno, A.M.L. Lanzolla, M. Spadavecchia, V.L. Scarano, "Camera calibration procedure to improve safety in railway tunnel" in *20th IMEKO TC4 Symposium on Measurements of Electrical Quantities; Together with 18th TC4 International Workshop on ADC and DCA Modeling and Testing, IWADC 2014*, pp. 626-630.

[33] D. Türler, B. T. Griffith, D.K. Arasteh, " Laboratory Procedures for Using Infrared Thermography to Validate Heat Transfer Models," *Insulation Materials: Testing and Applications: Third Volume*, ASTM STP 1320, 1997

[34] Wen-Hwa Chen, Hsien-Chie Cheng and Hsin-An Shen, "An effective methodology for thermal characterization of electronic packaging," in *IEEE Transactions on Components and Packaging Technologies*, vol. 26, no. 1, pp. 222-232, March 2003. doi: 10.1109/TCAPT.2002.806180

[35] L. Ciani, M. Catelani, E. A. Carnevale, L. Donati, M. Bruzzi, "Evaluation of the ageing process of Dye-Sensitized Solar Cells under different stress conditions", *IEEE Transactions on Instrumentation and Measurement*, vol.64, no.5, pp.1179,1187, May 2015, doi: 10.1109/TIM.2014.2381352

[36] X. Perpiñà, R. J. Werkhoven, M. Vellvehi, J. Jakovenko, X. Jord`a, J. M. G. Kunen, P. Bancken, and P. J. Bolt, "Thermal Analysis of LED Lamps for Optimal Driver Integration," in *IEEE Transactions on Power Electronics*, vol. 30, no. 7, pp. 3876-3891, July 2015. doi: 10.1109/TPEL.2014.2346543

[37] M. Catelani, L. Ciani, L. Cristaldi, M. Faifer, M. Lazzaroni, "Electrical performances optimization of Photovoltaic Modules with FMECA approach", *Measurement*, Volume 46, Issue 10, December 2013, Pages 3898 - 3909, ISSN 0263-2241, doi: j.measurement.2013.08.003

[38] M. Catelani, L. Ciani, "Experimental tests and reliability assessment of electronic ballast system", *Microelectronics Reliability*, Volume 52, Issues 9–10, September–October 2012, Pages 1833-1836, ISSN 0026-2714, 10.1016/j.microrel.2012.06.077

[39] M. T. Barako, Woosung Park, A. M. Marconnet, M. Asheghi and K. E. Goodson, "A reliability study with infrared imaging of thermoelectric modules under thermal cycling," *13th IEEE Intersociety Conference on Thermal and Thermomechanical Phenomena in Electronic Systems (ITherm)*, 2012, San Diego, CA, 2012, pp. 86-92. doi: 10.1109/ITHERM.2012.6231417

[40] The Ultimate Infrared Handbook for R&D Professionals, FLIR

[41] S. Marinetti, P. G. Cesaratto, "Emissivity estimation for accurate quantitative thermography", *NDT & E International*, Volume 51, October 2012, Pages 127-134, ISSN 0963-8695, doi: 10.1016/j.ndteint.2012.06.001

[42] W. Minkina, S. Dudzik, "Infrared Thermography: Errors and Uncertainties", *John Wiley & Sons*, Ltd, Chichester, UK, 2009, pp. 23-25, doi: 10.1002/9780470682234.ch2

[43] http://www.thermonamic.com/TES1-12730-NET1.pdf

[44] FLIR ResearchIR 4, Online: http://www.flir.com/science/display/?id=66484

[45] Loss Function and Model Quality Metrics, Online: http://it.mathworks.com/help/ident/ug/model-quality-metrics.html

[46] Use low-cost materials to increase target emissivity, FLIR Research & Science, online: http://www.flir.com/science/blog/details/?ID=71556

LIST OF FIGURES

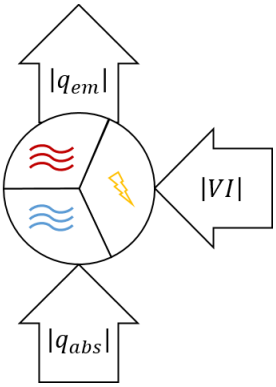

Fig. 1 - Concept diagram of a heat engine

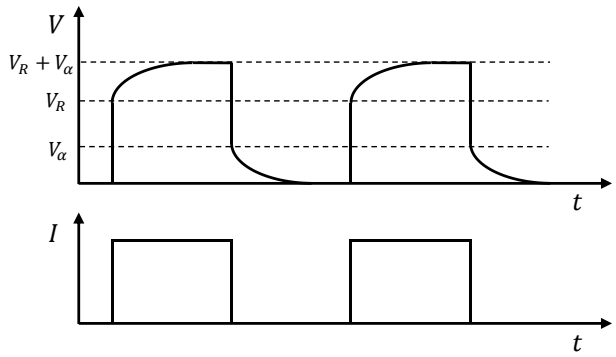

Fig. 2 - Typical TEM voltage profile using transient method: applied current *I* (bottom) and resulting voltage *V* (top) vs. time.

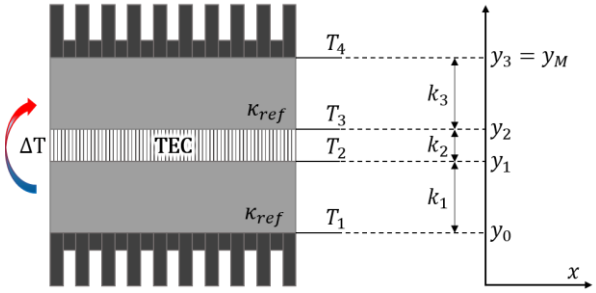

Fig. 3 – General scheme for the measurement of the thermal resistance Θ

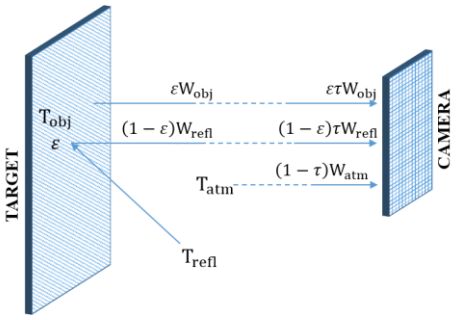

Fig. 4 - Total incident power contributions

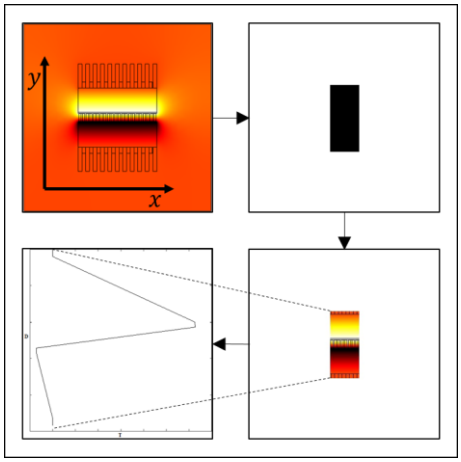

Fig. 5 - Example of measurement mask applied to a TEC simulation in COMSOL Multiphysics

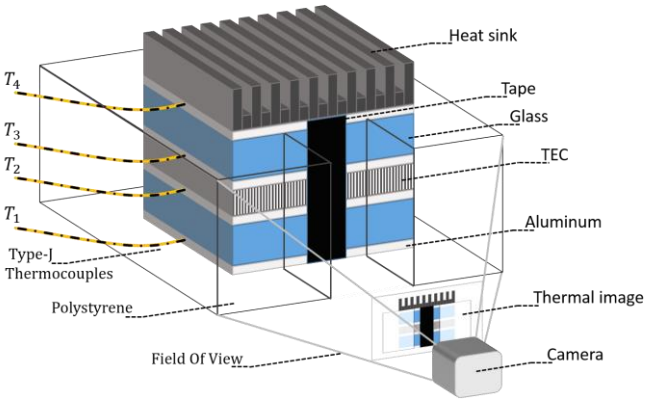

Fig. 6 - Measurement setup for thermal imaging method validation

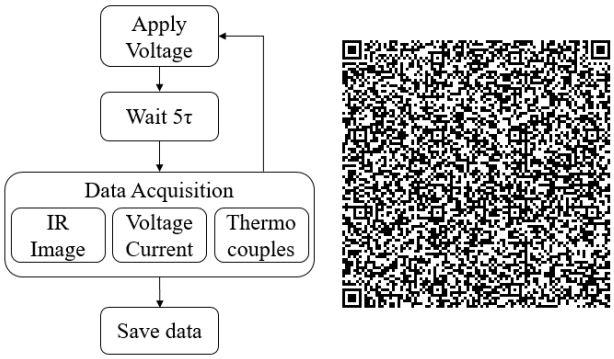

Fig. 7 - Measurement flow-chart (left); MATLAB/FLIR robot code (right)

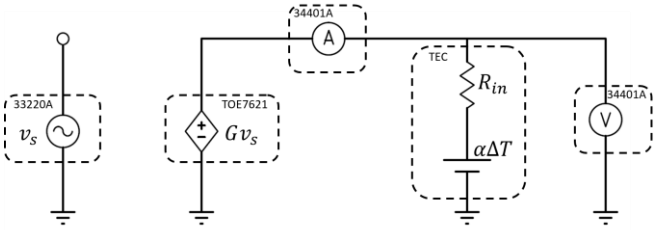

Fig. 8 - Electrical measurement setup

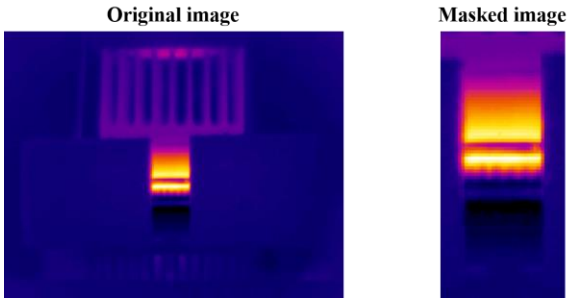

Fig. 9 - Original thermal image and extracted mask for $I = 0.615\ A$

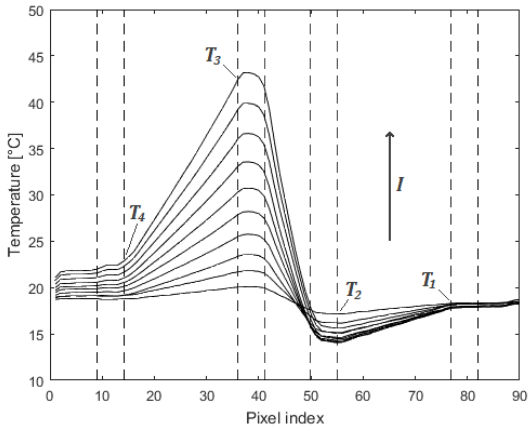

Fig. 10 - Temperature profiles (solid lines) and layer interfaces (dashed lines)

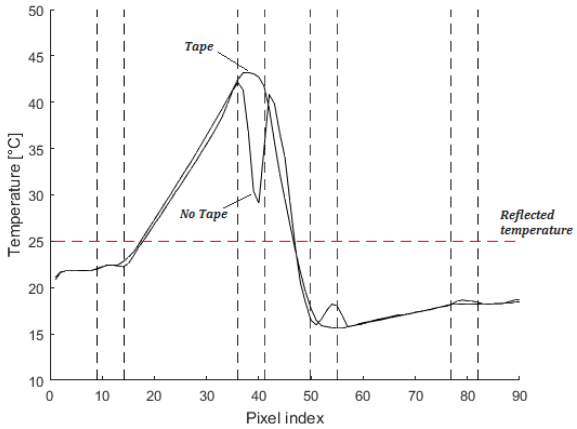

Fig. 11 - Effect of electrical tape on temperature estimation for $I = 0.615\ A$

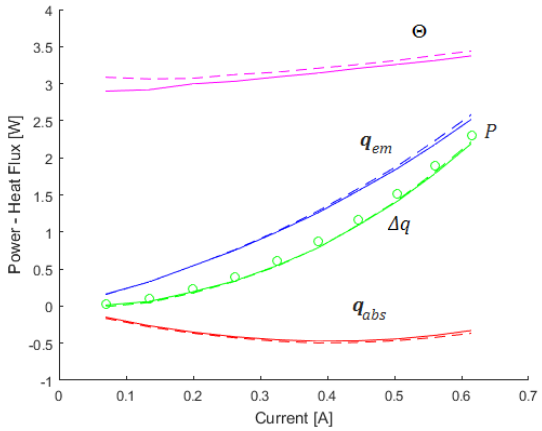

Fig. 12 - Results from thermocouples based method (dashed lines) vs. thermal imaging method (solid line). The electrical power is marked with circles.

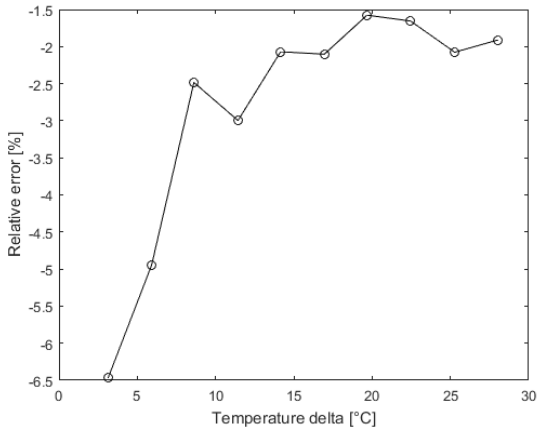

Fig. 13 - Thermal resistance relative error of thermal imaging based method with respect to thermocouples based method

LIST OF TABLES

TABLE I.TES1-12730 PARAMETERS

Symbol	Description	Value	
n	Number of thermocouples	127	
	Single module size [mm] x [mm]	30x30	
T_h	Hot side temperature at environment [°C]	27	50
ΔT_{max}	Temperature Difference when cooling capacity is zero at cold side [°C]	68	76
V_{max}	Voltage applied to the module at ΔT_{max} [V]	15.5	17.4
I_{max}	DC current through the modules at ΔT_{max} [A]	3.5	3.5
$Q_{c_{max}}$	Cooling capacity at cold side of the module under $\Delta T = 0$ °C [W]	34.1	37.4
R_{in}	Module resistance under AC [Ω]	3.5~3.9	3.8~4.3
R_{ds}	Internal resistance [A] [Ω]	3.42	3.79
α_{ds}	Seebeck coefficient [A] [mV/K]	51.7	53.7
Θ_{ds}	Thermal resistance [A] [W/K]	3.24	3.27

[A] Parameters extracted from datasheet using procedure in [19]

TABLE II. SETUP PARAMETERS

Symbol	Description	Value
h_{cer}	Ceramic module surface thickness [mm]	0.5
h_{alu}	Aluminum layer thickness [mm]	2
h_{TEC}	TEC module thickness [mm]	3.7
h_{glass}	Glass layer thickness [mm]	8
κ_{alu}	Aluminum thermal conductivity [$W/m \cdot K$]	237
κ_{glass}	Glass thermal conductivity [$W/m \cdot K$]	1.1
κ_{cer}	Ceramic thermal conductivity [$W/m \cdot K$]	30
A	Module area [mm^2]	30x30
d	Distance of the camera from the setup [cm]	30
ε_{cal}	Calibration emissivity value	0.92

TABLE III. PRECISION COMPARISON

Symbol	Description	Standard Deviation σ Thermo-couple	Thermal Imaging
I	Current [mA]	0.763	
V	Voltage [mV]	0.215	
P	Power [mW]	2.737	
T_1	Temperature T_1 [°C]	0.112	0.145
T_2	Temperature T_2 [°C]	0.201	0.233
T_3	Temperature T_3 [°C]	0.199	0.236
T_4	Temperature T_4 [°C]	0.093	0.161
q_{em}	Emitted heat flux [mW]	15.54	14.64
q_{abs}	Absorbed heat flux [mW]	15.48	17.98
Δq	Heat flux difference [mW]	30.62	32.34
Θ	Thermal resistance [°C/mW]	9.854	11.235

[A]Statistics are computed over a measurement sample size equal to 90

LIST OF FIGURE CAPTIONS

LIST OF TABLE TITLES

SHORT BIOGRAPHIES

Filippo Attivissimo received the M.S. and the Ph.D. degrees in Electronic Engineering from the Polytechnic of Bari, Italy, in 1993 and 1997 respectively. He is an Associate Professor of Electronic Measurements with the Department of Electrical and Information Engineering of the same Polytechnic. His current research interests include digital signal processing, development and characterization of sensors for environmental applications and renewable energies, power quality systems and measurements for medical applications. He is member of the IEEE I&M Society and of the Italian Group of Electrical and Electronic Measurements (GMEE)."

Attilio Di Nisio (M '14) was born in Bari, Italy, in 1980. He received the M.S. (Hons.) degree and the Ph.D. degree in electronic engineering from Politecnico di Bari, Bari, in 2005 and 2009, respectively, where he is currently a Research Assistant. Since 2005, his research spanned the fields of analog-to-digital and digital-to-analog converters modeling and testing, estimation theory, software for automatic test equipment, sensors, image processing for medical and quality control applications, photovoltaic and thermoelectric modules modeling and testing. His current research interests include DSP-based systems for power quality analysis, wireless sensor networks and soil mechanics testing equipment. Dr. Di Nisio is a member of the Italian association Electrical and Electronic Measurements Group.

Carlo Guarnieri Calò Carducci received the M.S. degree in electronics engineering from the Polytechnic of Bari, Bari, Italy, in 2013. In the same year he received a scholarship and he is currently working towards the Ph.D. degree at the Department of Electrical and Information Engineering. His current research interests include environmental sensor design, wireless sensor networks and energy harvesting.

Maurizio Spadavecchia (S'11-M'14) received his MS degree with honors and his PhD in Electrical Engineering from the Politecnico di Bari in 2006 and 2011, respectively. Since 2006, he was with the Electrical and Electronic Measurements Laboratory of the Politecnico di Bari where he is a Research Fellow. His current research interests include electrics and electronics measurement on instruments and devices, characterization of renewable energies devices, software for automatic test equipment, photovoltaic and thermoelectric modules modeling and testing and power quality systems and measurements, smart metering and soil mechanics testing equipment. He is a member of the IEEE Instrumentation and Measurements society and of the Italian association Electrical and Electronic Measurements Group.